JOURNAL OF MATERIALS SCIENCE 25 (1990) 4745–4751

# Effect of microstructure on tensile fracture of quenched and lightly tempered high carbon and low chromium steel containing undissolved spheroidal carbides

YOSHIYUKI TOMITA
*Department of Metallurgical Engineering, College of Engineering, University of Osaka Prefecture, 4-804 Mozu-Umemachi, Sakai, Osaka 591, Japan*

High carbon and low alloy chromium steels have been studied to determine the effect of the microstructure on tensile fracture of quenched and lightly tempered low alloy steel containing undissolved spheroidal carbides. The steels with a volume fraction of 8 and 13 vol% and containing particle sizes from 0.32 to 1.14 $\mu$m were investigated. In the case of steel containing 8 vol% undissolved carbides, many twinned plates were observed in the matrix martensite and microtwinning was observed in the carbide/matrix interfaces. The steel failed in a macroscopically brittle manner and the true fracture stress of the steel was independent of the carbide particle size, while the data exhibited a large scatter. In the case of steel containing 13 vol% of undissolved carbides, the matrix martensite consisted predominantly of lath martensite and a well-defined forest of dislocations was observed around the carbides. Failure of the steel occurred in the relatively early stage of plastic deformation and the true fracture stress of the steel increased with decreasing carbide particle size.

## 1. Introduction

Iron and alloy carbides undissolved during austenitization can have marked effects on mechanical properties and fracture behaviour of heat-treated structural low alloy steels [1, 2]. However, there has been little systematic study made of the correlation of the microstructure and fracture behaviour of the steel containing the undissolved carbides, while there have been many studies made of the effect of microstructure on plastic deformation and fracture behaviour of ferritic steels containing spheroidal or rod-shaped carbides [3–12]. Thus, a fundamental programme was initiated to understand the correlation between the microstructure and fracture behaviour of the steels with undissolved spheroidal carbides.

Much of the past work concerning quenched and lightly tempered low alloy steels containing undissolved spheroidal carbides had related microstructural features to rolling contact fatigue performance, in view of bearing application of the steels. For example, finer carbides produce improved bearing fatigue life [13] and oxide inclusion particles are significantly more detrimental to fatigue life than are sulphides [14]. Rolling contact fatigue produces very fine microstructural changes observable as etching effects under an optical microscope [15]. More recently, these effects in AISI 52100 steel have also been observed in transmission electron microscopic studies [16, 17], which characterized three types of structure resulting from martensite and carbides decaying under cyclic stress. Little information exists, however, on fracture behaviour of the steels.

In the present work, high carbon and low chromium steels have been studied to determine the effect of the microstructure on tensile fracture of quenched and lightly tempered alloy steels containing the undissolved spheroidal carbides.

## 2. Experimental procedure

Two high carbon and low chromium steels were used in this investigation. The chemical composition of the steels along with gas analysis and cleanliness is given in Table I. The steels were prepared as $30 \times 10^3$ kg vacuum degassed heats. The ingots ($2.5 \times 10^3$ kg) were hot rolled to 80 mm diameter at a temperature of 1473 K and above. Steel A was used to determine the effect of undissolved carbides on tensile fracture while steel B was used for studying the effect of the matrix

TABLE I Chemical composition (wt%), gas analysis (p.p.m.) and cleanliness (%) of steels used

| Steel | C | Si | Mn | P | S | Cr | Ni | Cu | O | N | H | $d_A$ % | $d_B$ % | $d_C$ % |
|---|---|---|---|---|---|---|---|---|---|---|---|---|---|---|
| Steel A | 1.08 | 0.20 | 0.38 | 0.005 | 0.013 | 1.40 | 0.03 | 0.05 | 16.0 | 20.1 | 1.3 | 0.02 | 0.01 | 0.002 |
| Steel B | 0.60 | 0.22 | 0.30 | 0.006 | 0.012 | 0.81 | 0.02 | 0.05 | 15.8 | 19.3 | 1.5 | 0.02 | 0.02 | 0.002 |

0022–2461/90 $03.00 + .12 

TABLE II Heat-treatment schedule for obtaining 8 vol % carbide steels

| Designation of steel | | Heat treatment |
|---|---|---|
| (I) | Steel containing fine carbide | Austenitize at 1113 K for 720 sec, interrupted quench at 523 K for 5 sec, oil quench, subzero-treat at 77 K for 72 ksec, double-temper for 3.6 ksec per temper at 473 K. |
| (II) | Steel containing intermediate carbide | Austenitize at 1113 K for 900 sec, interrupted quench at 523 K for 5 sec, oil quench, subzero-treat at 77 K for 72 ksec, double-temper for 3.6 ksec per temper at 473 K. |
| (III) | Steel containing coarse carbide | Austenitize at 1113 K for 1560 sec, interrupted quench at 523 K for 5 sec, oil quench, subzero-treat at 77 K for 72 ksec, double-temper for 3.6 ksec per temper at 473 K. |

martensite on tensile fracture. Test steels were cut in the longitudinal orientaton for the bars. Each steel was spheroidized and subsequently heat-treated. The spheroidizing–anneal schedule and the heat treatment schedule is given in Fig. 1 and Tables II and III, respectively. All test steels were spheroidizing–annealed in a vacuum furnace. Austenitization was done in a lead bath. The interrupted quenching treatments at 523 or 623 K just above the $M_s$ temperature, whereby the mass effect can be neglected through the heat treatments, were done in a lead–tin bath. Both baths had sufficient thermal capacity. After quenching, all test steels were immersed in liquid nitrogen and refrigerated for about 72 ksec. The steels were double tempered for 3.6 ksec per temper at 473 K in an oil bath. This was done to eliminate retained austenite as much as possible. Tensile tests were performed using tensile specimens as shown in Fig. 2. The final dimension of the gauge were obtained by careful grinding. The specimens were pulled on an Instron machine at ambient temperature (293 K) at a constant strain rate of $6.70 \times 10^{-4}\ \text{sec}^{-1}$.

The microstructure was categorized using optical and thin-foil transmission electron microscopy (TEM). Thin-foils were prepared from the ends of the tensile specimens, first by mechanical grinding to 0.1 mm thickness, then by chemical thinning in a mixed solution of hydrofluoric acid and hydrogen peroxide. Finally, the specimens were electropolished in a mixed solution of phosphoric and chromic acids. The volume fraction of the undissolved spheroidal-carbides and their mean particle size were determined from micrographs by two-stage cellulose acetate–platinum shadowed carbon replicas using TEM. The volume fraction of the carbides was determined by the ASTM linear analysis method. Between 1300 and 1500 carbides on the micrographs were taken at random to measure the mean particle size. The mean carbide particle size, $\bar{d}$, is given by [18]

$$\bar{d} = (\pi/2)(\Sigma n_i d_i / \Sigma n_i) \quad (1)$$

where $d_i$ is the diameter of undissolved spheroidal carbides appearing on the micrographs and $n_i$ is the frequency with which they appear. Prior austenite grain size was determined by the ASTM linear analysis method with an optical microscope using specimens etched with a supersaturated aqueous solution of picric acid containing 0.2 wt % surface agent [19, 20]. In order to determine quantitatively the carbon, chromium and manganese contents in the matrix, undissolved carbides were separated electrolytically at a current density of 100 mA using 0.5 N hydrochloric acid. Fracture morphology was characterized by two-stage cellulose acetate–platinum shadowed carbon replicas using TEM. Quantitative analysis of the retained austenite was made by X-ray diffraction measurements using the step scan operated at 0.025° $\text{sec}^{-1}$ with Co$K\alpha$ radiation [21].

## 3. Results

### 3.1. Microstructure

Mean carbide particle size, $\bar{d}$, prior austenite grain size, $d_\gamma$, and the amount of retained austenite of the 8 and 13 vol % carbide steel A are listed in Table IV. The significant observations are as follows. (1) The mean particle size of the 8 and 13 vol % carbide steels

TABLE III Heat-treatment schedule for obtaining 13 vol % carbide steels

| Designation of steel | | Heat treatment |
|---|---|---|
| (I) | Steel containing fine carbide | Austenitize at 1113 K for 480 sec, interrupted quench at 623 K for 5 sec, oil quench, subzero-treat at 77 K for 72 ksec, double-temper for 3.6 ksec per temper at 473 K. |
| (II) | Steel containing intermediate carbide | Austenitize at 1113 K for 600 sec, interrupted quench at 623 K for 5 sec, oil quench, subzero-treat at 77 K for 72 ksec, double-temper for 3.6 ksec per temper at 473 K. |
| (III) | Steel containing coarse carbide | Austenitize at 1113 K for 900 sec, interrupted quench at 623 K for 5 sec, oil quench, subzero-treat at 77 K for 72 ksec, double-temper for 3.6 ksec per temper at 473 K. |

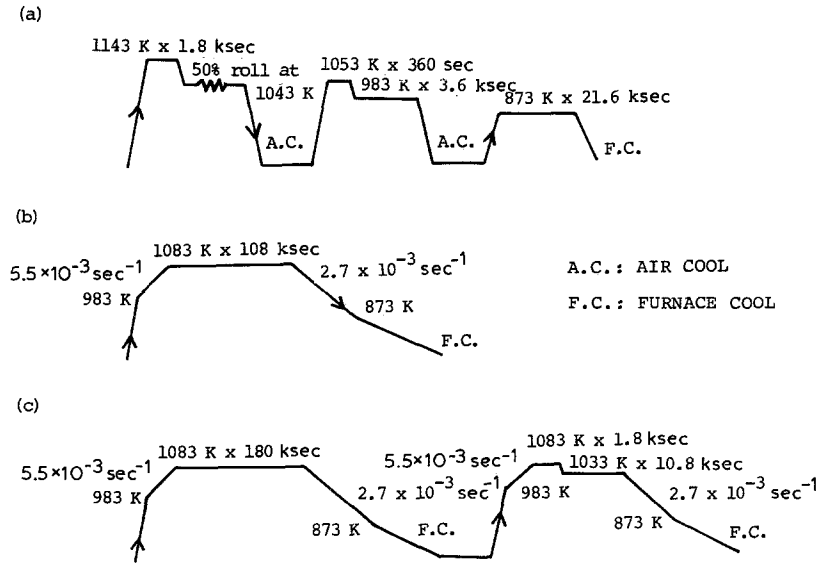


*Figure 1* Schematic diagrams of spheroidizing treatment of carbides. (a), (b) and (c) indicate spheroidizing treatment for obtaining fine, intermediate and coarse carbides, respectively.

varied from 0.32 to 0.83 $\mu$m and from 0.41 to 1.14 $\mu$m, respectively. (2) Prior austenite grain size increased somewhat as the mean carbide size increased. However, the difference was not extreme. (3) The amount of retained austenite is almost independent of the mean carbide size at the same volume fraction level.

Figs 3 and 4 show representative TEM micrographs from the steels. The results obtained are summarized as follows. (1) In the case of 8 vol % carbide steel, twinned plates were observed in the matrix martensite independent of carbide particle size (arrow A in Fig. 3a). Microtwinning was obsreved at the interfaces of the carbide/matrix independent of particle size (arrow B in Fig. 3b). This could be due to a marked difference between cubical expansion of the matrix and the carbide during martensitic transformation. (2) In the case of 13 vol % carbide steels, the martensite consisted predominantly of lath martensite. A well-defined forest of dislocations was observed around the carbides independent of particle size. The above alteration of martensitic morphology can be attributed to the fact that the carbon content dissolved in the matrix martensite is changed by the amount of undissolved carbide. Table V shows typical carbon, chromium and manganese contents in the matrix that were electrolytically determined. The results are summarized as follows. (1) For the 8 vol % carbide steel, carbon and chromium contents in the matrix were, respectively, 0.60 to 0.63 wt % and 0.78 to 0.82 wt %, independent of the particle size of the carbide. (2) For the 13 vol % carbide steel, the carbon and chromium contents were, respectively, 0.43 to 0.45 wt % and 0.67 to 0.69 wt %, independent of the particle size of the carbide. (3) The manganese content was 0.30 to 0.32 wt %, independent of the volume fraction of the carbides.

## 3.2. Mechanical test

Tensile properties of the steels are given in Table VI. As can be seen from this table, the tensile fracture behaviour of the steels fell into two categories. (1) The 8 vol % carbide steel failed in a macroscopically brittle manner (within elastic limit) and the true fracture

TABLE IV Microstructural parameters of steels containing 8 and 13 vol % undissolved spheroidal carbide

| Designation of steel containing carbide | | Mean particle size of carbide, $\bar{d}$ ($\mu$m) | Vickers hardness ($H_v$) | Prior austenite grain size, $d_\gamma$ ($\mu$m) | Content of retained austenite (vol %) |
|---|---|---|---|---|---|
| 8 vol % steel: | fine carbide | 0.32 | 850 | 6.7 | 2.0 |
| | intermediate carbide | 0.43 | 845 | 7.2 | 1.8 |
| | coarse carbide | 0.83 | 852 | 7.7 | 1.7 |
| 13 vol % steel: | fine carbide | 0.41 | 810 | 6.5 | < 1.5 |
| | intermediate carbide | 0.62 | 805 | 6.8 | < 1.5 |
| | coarse carbide | 1.14 | 813 | 7.1 | < 1.5 |

TABLE V Alloying element contents dissolved in matrix martensite

| Designation of steel containing carbide | | C (wt %) | Cr (wt %) | Mn (wt %) |
|---|---|---|---|---|
| 8 vol % steel: | fine carbide | 0.63 | 0.80 | 0.30 |
| | intermediate carbide | 0.62 | 0.78 | 0.31 |
| | coarse carbide | 0.60 | 0.82 | 0.31 |
| 13 vol % steel: | fine carbide | 0.45 | 0.68 | 0.32 |
| | intermediate carbide | 0.43 | 0.67 | 0.30 |
| | coarse carbide | 0.45 | 0.69 | 0.30 |

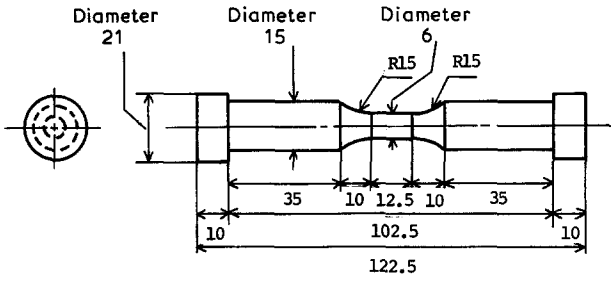


*Figure 2* Dimensions (in mm) of tensile specimens used.

stress ($\sigma_f$) of the 8 vol % carbide steel was in the range 990.8 to 1190.6 MPa, independent of the carbide particle size, while the data exhibited a large scatter. (2) Failure of the 13 vol % carbide steels occurred in the relatively early stage of plastic deformation, independent of carbide particle size, while $\sigma_f$ of the steel exceeds 0.2% yield stress, independent of carbide particle size, and $\sigma_y$ increased with decreased carbide particle size.

### 3.3. Fractography

It is well known that fractography directly describes the situation of the fracture process and provides valuable evidence concerning the cause of failure. Therefore, a careful examination of the fracture appearance was made of the broken surface of steel A. Typical results are shown in Figs 5 and 6. Different fracture modes were observed in the 8 and 13 vol % carbide steels. Fractography revealed that for the 8 vol % carbide steel a characteristic river pattern radiating from the carbide/matrix interfaces was observed, independent of the carbide particle size (arrow in Fig. 5). Fractography also revealed that for the 13 vol % carbide steel crack nucleation occurred either by cracking of the carbide particles or separation at the carbides/matrix interfaces (arrow in Fig. 6). The above results suggest that for the 8 vol % carbide steel failure occurs by a crack propagating from the carbide/matrix interfaces and that failure of the 13 vol % carbide steel occurred by connection of microcracks which were initiated by separation (cracking) of the carbides from matrix.

## 4. Discussion

It can be seen from the present investigation that the effect of the microstructure on tensile fracture of quenched and lightly tempered steels containing undissolved spheroidal carbides fall into two categories. One is that failure of 8 vol % carbide steels occurs in a macroscopically brittle manner and the true fracture stress is independent of the particle size of the carbide. The other is, that 13 vol % carbide steels failed in the relatively early stage of plastic deformation, while they exceeded yield stress and that the true fracture stress increased with decreased carbide particle size. In this section, the above results are briefly discussed.

### 4.1. 8 vol % carbide steel

On the basis of the results from metallographic observation, fractography, and the fact that fracture occurred in a macroscopically brittle manner (within the elastic limit), the effect on fracture for the 8 vol % carbide steels is thought to be controlled by the stress concentration in the carbide/matrix interfaces. This could be due to the fact that great residual stress remains or microcracks were introduced at the carbides/matrix interfaces after quenching because tensile stress was produced in the carbides and compressive stress in the matrix closest to the interfaces of the carbide/matrix when the steel was quenched. This is assumed from the results in Fig. 3. On the basis of the above idea, the following relation between the microstructure and fracture stress, $\sigma_f$, was derived. When tensile stress is applied through the steel containing hard inclusions or precipitates, the true stress, $\sigma_f$, is given by [22]

$$\sigma_f = \sigma_m/\alpha \quad (2)$$

where $\sigma_m$ is the true fracture stress in the matrix closest to the interfaces of the inclusions/matrix or precipitates/matrix and $\alpha$ is the stress concentration factor at the interfaces. It has generally been recognized that $\alpha = 3$ in the steel with mechanical circular holes independent of the diameter of the hole when uniaxial stress is applied. However, it would be unjust to apply this value to the present investigation because the order of the size is quite different. Therefore, the high stress concentration factor in the inclusions/matrix interfaces proposed by Goodies [23] was applied because it is considered to be of the same order of the value of the carbide/matrix interfaces. He has shown that when uniaxial stress is applied in the matrix with a rigid inclusion, the stress concentration factor estimated in the inclusion/matrix is given by

$$\alpha = (27 - 15\nu)/(14 - 10\nu) \quad (3)$$

where $\nu$ is Poisson's ratio. When $\nu$ is 0.3, $\alpha$ becomes approximately 2.05. As listed in Table V, the carbon, chromium and manganese contents of the matrix in the 8 vol % carbide steel are, respectively, about 0.6, 0.8 and 0.3 wt %, independent of particle size of the carbide. So, in order to estimate $\sigma_m$, three steel B specimens with similar carbon, chromium and manganese

TABLE VI Tensile properties of steels A and B. Results are the mean of five measurements

| Designation of steel containing carbide | | Mean particle size of carbide ($\mu$m) | 0.2% yield stress, $\sigma_y$ (MPa) | True fracture stress, $\sigma_f$ (MPa) | Total elongation (%) |
|---|---|---|---|---|---|
| 8 vol % steel: | fine carbide | 0.32 | – | 1155.8 | Not evaluated |
| | intermediate carbide | 0.43 | – | 1290.6 | Not evaluated |
| | coarse carbide | 0.83 | – | 1210.3 | Not evaluated |
| 13 vol % steel: | fine carbide | 0.41 | 1820.6 | 1848.2 | 2.9 |
| | intermediate carbide | 0.62 | 1790.6 | 1816.5 | 2.6 |
| | coarse carbide | 1.14 | 1750.2 | 1780.3 | 2.3 |

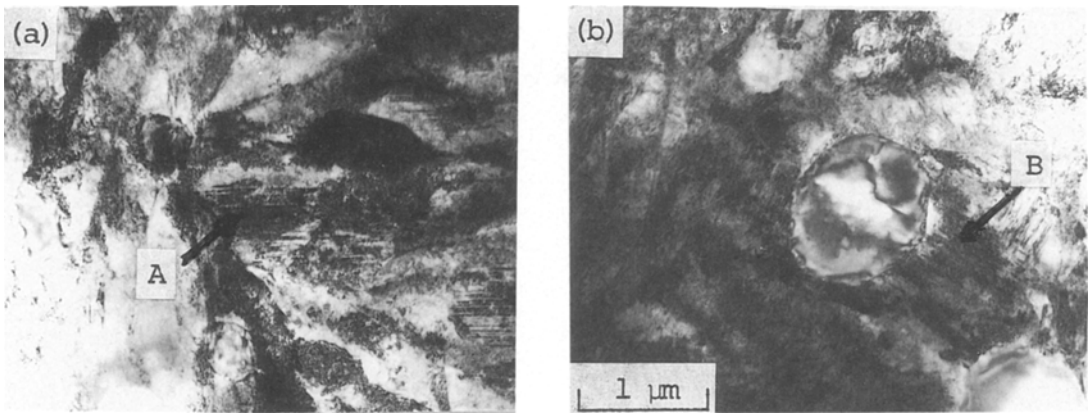


*Figure 3* Transmission electron micrographs of steel containing 8 vol % undissolved (a) fine and (b) coarse spheroidal carbides, heat-treated by schedules (a) I and (b) III in Table II. Arrows A on (a) and (b) indicate twinned plates in matrix martensite. Arrow B in (b) indicates microtwinning formed at the carbide/matrix interface.

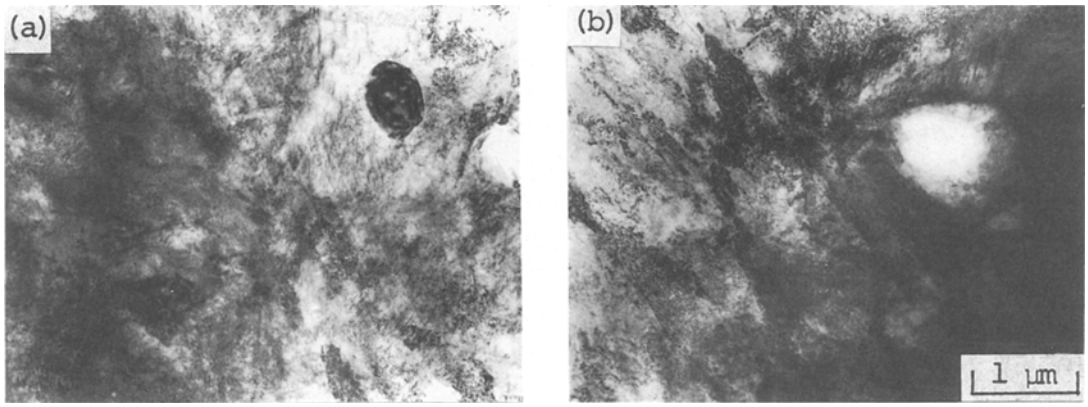


*Figure 4* Transmission electron micrographs of steels containing 13 vol % of undissolved (a) fine and (b) coarse spheroidal carbides, heat-treated by schedules (a) I and (b) III in Table III.

were pulled using an Instron machine. The value of the $\sigma_m$ obtained was 1580.6 to 1620.8 MPa. Substituting $\sigma_m$ = 1580.6 to 1620.8 MPa and $\alpha$ = 2.05 in Equation 2 we obtained $\sigma_f$ = 771.0 to 790.6 MPa. As can be seen from comparison of the results with measured fracture stress (1155.8 to 1290.6 MPa) as shown in Table VI, the calculated values of $\sigma_f$ are the same order as the measured data, while the measured data are somewhat higher than the calculated values. From these results, it is postulated that the fracture stress of 8 vol % carbide steels is controlled by the high stress concentration in the carbide/matrix interfaces.

### 4.2. 13 vol % carbide steel

From the present results, the effect of the microstructure on tensile fracture of 13 vol % carbide steels during tensile testing is considered to consist of three parts: (1) plastic deformation of the matrix, (2) microcrack nucleation either by cracking of the carbide particles or separation at the carbides/matrix interfaces in the relatively early stage of plastic deformation (work hardening), and (3) the joining of the microcracks produced by these failures or separation through release of the elastic stored energy, producing the final fracture. On the basis of the fact that the

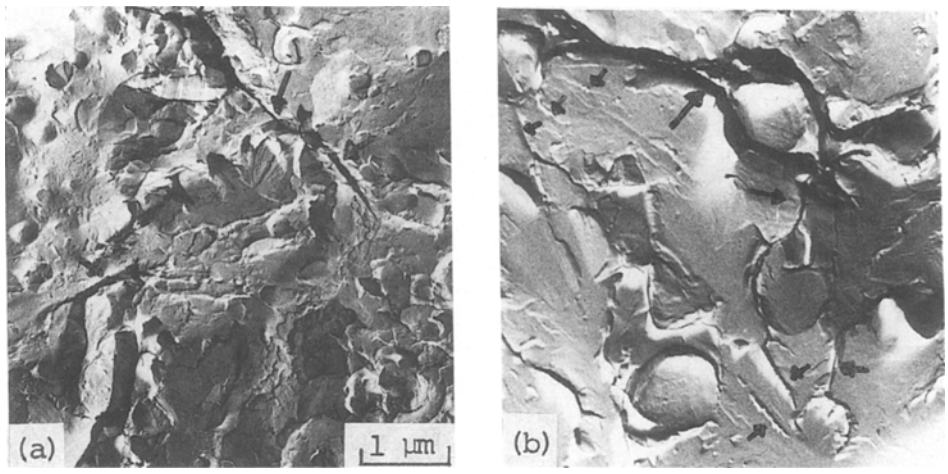


*Figure 5* TEM fractographs of 8 vol % carbide steels, heat-treated by schedules (a) I and (b) III in Table II, respectively. Arrows on (a) and (b) indicate river patterns radiating from carbide/matrix interfaces.

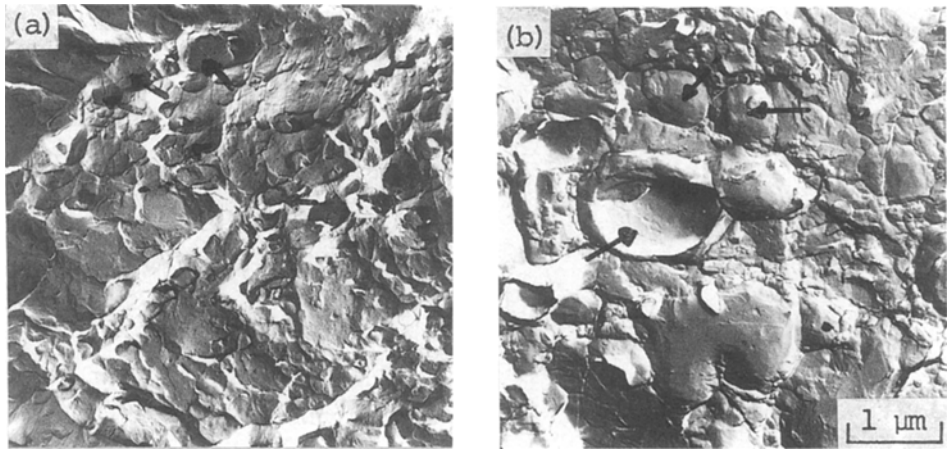


*Figure 6* TEM fractographs of 13 vol % carbide steels, heat-treated by schedules (a) I and (b) III in Table III, respectively. Arrows on (a) indicate microcracks seeming to initiate at separation or cracking of carbides during plastic deformation.

above sequence occurs in a relatively early stage in plastic deformation (work hardening), the relation between microstructure and fracture was derived from the theory of Fisher *et al.* [24] for the strengthening due to dispersions. When dislocations of $N$ loops are piled up around the carbide particles, the applied stress, $\sigma$, required for activating Frank–Read's source around a carbide particle is approximated by

$$\sigma = \mu \boldsymbol{b} N/R\mathrm{m}(r/R)^2 \quad (4)$$

where $r$ is the mean radius of the sections of the carbide particles in the slip plane, $2R$ is the mean spacing between the particles, $R$m is the distance of closest approach of a source to the particle, $\mu$ is the rigid modulus of the matrix, and $\boldsymbol{b}$ is the Burgers vector. When $R\mathrm{m} = R/3$, Equation 4 becomes

$$\sigma = 3\mu(r/R)^3(N\boldsymbol{b}/r) \quad (5)$$

The strain energy of a pile-up of dislocations against the particle/matrix interface is approximately equal to $\mu N^2\boldsymbol{b}^2$ [3]. Therefore, using Equation 5, the strain energy is given by

$$\mu N^2\boldsymbol{b}^2 = \sigma^2/9\mu(r/R)^6(1/r^2) \quad (6)$$

When a crack opens in a particle, the strain energy is converted to surface energy. That is, when $\mu N^2\boldsymbol{b}^2 = 4\gamma r$, Equation 6 becomes

$$\sigma = 6(\gamma\mu)^{1/2}(r/R)^3(1/r^{1/2}) \quad (7)$$

where $\gamma$ is the surface energy. If $f$ is the volume fraction of the carbide, $R$ is given by [4, 18]

$$R = 2\gamma[(1 - f)(2/3f + 1)^{1/2}]/2 \quad (8)$$

Substituting Equation 8 for $R$ in Equation 7 one obtains

$$\sigma = 6(\gamma\mu)^{1/2}[1/(1 - f)(2/3f + 1)^{1/2}]^3(1/r^{1/2}) \quad (9)$$

Thus, if $\sigma$ equals to $\sigma_f$ and $f$, $\gamma$ and $\mu$ are constant, $6(\gamma\mu)^{1/2}[1/(1 - f)(2/3f + 1)^{1/2}]^3 = k$ (constant) and thus, if $r = \bar{d}/2$, Equation 9 becomes

$$\sigma_f = k(2/\bar{d})^{1/2} \quad (10)$$

where $d$ is the mean carbide particle size. Then, Equation 10 becomes

$$\sigma_f = k'/\bar{d}^{1/2} \quad (11)$$

where $k'$ is constant. In Fig. 7, the experimental true fracture stress, $\sigma_f$, is plotted against the parameter, $1/\bar{d}^{1/2}$. As can be seen from this figure, a fairly linear relation holds between $\sigma_f$ and $1/\bar{d}^{1/2}$. From the above results, the true fracture stress of the 13 vol % carbide steels follows a modified dispersion strengthening relation.

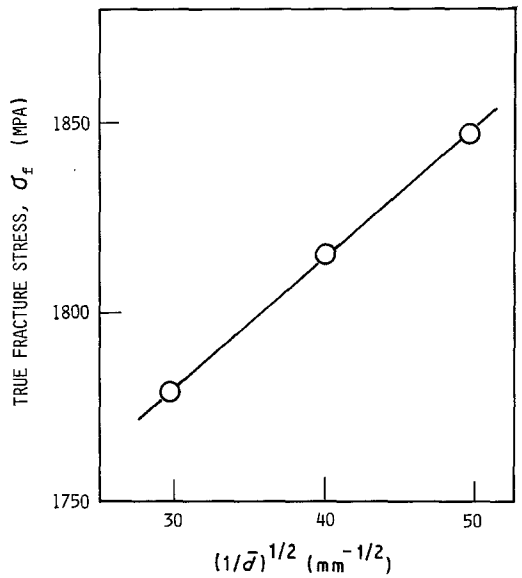


*Figure 7* Relationship between true fracture stress, $\sigma_f$, and $1/\bar{d}^{1/2}$ for 13 vol % carbide steels.

## 5. Conclusions

1. In steel containing 8 vol % undissolved carbides, many twinned plates were observed in the matrix martensite and microtwinning was observed at the carbide/matrix interfaces. The steel failed in a macroscopically brittle manner and the true fracture stress of the steel was independent of carbide particle size.

2. In steel containing 13 vol % undissolved carbides, the matrix consisted predominantly of lath martensite and a well-defined forest of dislocations was observed around the carbides. Failure of the steel occurred in the relatively early stage of plastic deformation. The true fracture stress of the steel increased with decreasing carbide particle size.

3. The results are briefly discussed in terms of stress concentration factor at the interfaces of the

carbide/matrix and modified dispersion strengthening relation.

## References


1. M. F. CARLSON, B. V. NARASHIMAHA and G. THOMAS, *Metall. Trans.* **10A** (1979) 1273.
2. S. LEE, L. MAJINO and R. J. ASARO, *Metall. Trans.* **16A** (1985) 1633.
3. W. W. WEBB and W. D. FORGENG, *Acta Metall.* **6** (1958) 462.
4. B. L. EDELSON and W. M. BALDWIN Jr, *Trans. ASM* **55** (1962) 230.
5. J. GURLAND, *Trans. TMS-AIME* **227** (1963) 1146.
6. C. J. McMAHON Jr and M. COHEN, *Acta Metall.* **13** (1965) 591.
7. J. T. BARNBY, *Acta Metall.* **15** (1967) 903.
8. J. T. LIU and J. GURLAND, *Trans. ASM* **61** (1968) 156.
9. T. C. LINDLEY, *J. Iron Steel Inst.* **207** (1969) 984.
10. T. GLADMAN, B. HOLMES and F. B. PICKERING, *ibid.* **208** (1970) 172.
11. A. CURRY and J. F. KNOTT, *Metal Sci.* **12** (1978) 511.
12. D. A. CURRY and P. L. PRATT, *Mater. Sci. Engng* **37** (1979) 223.
13. C. A. STICKEL, *Metall. Trans.* **5** (1974) 865.
14. C. M. LYNE and A. KASAK, *Trans. ASM* **61** (1968) 10.
15. J. BUCHWALD and R. M. HECKEL, *ibid.* **61** (1968) 750.
16. H. SWAHN, P. C. BECKER and O. VINGSBO, *Metal Sci.* **10** (1976) 35.
17. *Idem, Metall. Trans.* **7A** (1976) 1099.
18. R. L. FULLMAN, *Trans. TMS-AIME* **197** (1953) 447.
19. Y. TOMITA and K. OKABAYASHI, *Metall. Trans.* **17A** (1987) 1203.
20. Y. TOMITA, *ibid.* **18A** (1987) 1495.
21. J. DURNIN and K. A. RIDAL, *J. Iron Steel Inst.* **206** (1968) 60.
22. H. SUZUKI and K. HAYASHI, *J. Inst. Metal Jpn* **38** (1974) 1013.
23. GOODIES, *J. Appl. Mech. Trans. ASME* **55** (1933) 39.
24. J. C. FISHER, E. W. HART and R. H. PRY, *Acta Metall.* **1** (1953) 336.



*Received 6 June*
*and accepted 22 November 1989*